Determination of effective thermomechanical parameters of a mixture of two elastothermoviscoplastic constituents

B.M. Love *, R.C. Batra

Department of Engineering Science and Mechanics, Virginia Polytechnic Institute and State University, MC 0219, Blacksburg, VA 24061, USA

Abstract

We analyze plane strain deformations of a representative volume element (RVE) to evaluate effective thermophysical parameters of a particulate composite comprised of two perfectly bonded heat conducting elasto-thermo-visco-plastic constituents. It is assumed that the composite is also isotropic and its response elasto-thermo-visco-plastic. Effective values of material parameters so computed are compared with those obtained from either existing micromechanics models or the rule of mixtures or both. It is found that values computed from the rule of mixtures differ at most by 10% from those obtained by using the RVE. Effective stress versus effective strain curves obtained by analyzing simple shearing and axisymmetric deformations of the RVE and of the homogenized material, and also those obtained in plane strain deformations involving loading/unloading/reloading are found to be very close to each other. Time histories of the effective plastic strain at two neighboring points, one in each constituent, are quite different. The effective stress computed by the rule of mixtures from the average effective stress in each constituent and its volume fraction is very close to that obtained from surface tractions acting on the specimen boundaries. The average effective stress in a constituent is computed from the effective plastic strain averaged over that constituent. This also holds for a composite comprised of three constituents.
Published by Elsevier Ltd.

---

* Corresponding author.
E-mail addresses: brlove@vt.edu (B.M. Love), rbatra@vt.edu (R.C. Batra).

1. Introduction

Composites have become common engineering materials. The prospect of producing "designer" materials for specific applications is of great interest to many engineers. However, the thermomechanical behavior of these composites is more complex than that of homogeneous materials. Whereas continuous fiber-reinforced composites exhibit anisotropic material response, particulate reinforced composites are usually modeled as isotropic. Here, we are interested in particulate composites comprised of metallic particulates embedded in a metal matrix. Experimental testing to determine the thermophysical material parameters of a composite is tedious due to the increased number of material constants and the likelihood of unexpected nonlinearities and failure modes. Numerical simulation provides the ability to "test" a variety of composites under various loading conditions and help better understand the behavior of heterogeneous materials at both the micro- and the macro-scales. Since the micro-scale of many composites is far below reasonable length scales for macro-scale simulations, an accurate determination of bulk or "effective" properties that capture the overall behavior of the composite is highly desirable. Furthermore, failure modes and instabilities are not guaranteed to behave in the same way as in homogeneous materials – the heterogeneity of the material may cause interesting effects. Bridging the length scales between the macro-scale (at a length scale comparable to the material's application) and the micro-scale (at a length scale comparable to the microstructure of the material) allows one to investigate the effectiveness of the bulk properties to capture heterogeneity-driven phenomena. A better understanding of these phenomena is needed for critical uses of these materials.

Even though the techniques discussed and employed herein are applicable to any particulate composite, we focus on tungsten-heavy alloys (WHAs). WHAs are high density, high strength materials that are of interest in high strain-rate loading scenarios, most particularly, armor and armor-penetration applications. Due to the brittleness of pure tungsten, WHAs were developed to prevent brittle fracture/shattering under high stress; a typical WHA consists of tungsten particulates suspended in a nickel–iron matrix. The particulate is usually spherical and is randomly distributed; thus the overall response of the composite is isotropic. Unlike most composites, both constituents are capable of thermoelastoviscoplastic deformations – the tangent moduli of tungsten and nickel–iron are of the same order of magnitude, but their overall response when considering strain and strain-rate hardening, as well as thermal softening, are decidedly different.

Determination of effective properties of a composite from those of its constituents has been a topic of research for several decades. Much of the past work has been devoted to the determination of elastic and thermal constants of composites. Hashin

and Shtrikman (1963) established upper and lower bounds for the shear and the bulk modulus of a composite composed of several linear elastic phases. Mori and Tanaka (1973) developed the concept of average stress to account for the interaction among a finite concentration of linear elastic ellipsoidal particles embedded in a linear elastic matrix; Weng (1984) implemented this technique for isotropic constituents, giving closed form expressions for the shear modulus and the bulk modulus of the composite. Christensen and Lo (1979) built upon the three-phase model of Fröhlich and Sack (1946) and determined the effective shear modulus of a two constituent composite by examining the shear deformation of concentric spheres. Equating the strain energy of the composite sphere to the strain energy of the sphere comprised of the equivalent homogenized material with unknown properties allows for the analytical determination of the shear modulus; however, this method does not account for interaction among particulates. Nemat-Nasser and Hori (1993) have summarized different methods for the determination of elastic parameters of a composite. Jiang and Batra (2001a) used the mean-field theory and the Mori–Tanaka method to derive effective moduli of a three-phase composite comprised of a polymer matrix, and likewise oriented spherical and cylindrical shape memory alloy and piezoceramic inclusions. They (Jiang and Batra, 2001b) exploited the correspondence principle of linear viscoelasticity to evaluate effective moduli of a piezocomposite made of piezoceramic inclusions and a viscoelastic matrix. Subsequently, Jiang and Batra (2002) used the energy-equivalence principle and the Mori–Tanaka method to deduce effective thermo-electro-mechanical parameters of a 4-material composite consisting of an elastic matrix and shape memory alloy, piezoelectric and inert inclusions. It was shown that the shapes and the volume fractions of inert (e.g., air) inclusions significantly influenced the effective properties of the composite.

Estimation of the viscoplastic parameters of a composite is much more challenging. Suquet (1993) determined the upper and the lower bounds of the yield stress of a particulate composite composed of multiple incompressible power law materials. For a random dispersion of isotropic spherical particulates in an isotropic matrix, Suquet assumed that the compsite's response is also isotropic and derived an expression for the effective yield stress of the composite in terms of the yield stresses of the constituents and the effective shear modulus of the composite. Willis (1993) and Talbot and Willis (1985) established bounds for the stress–strain curve of a multi-phase nonlinear composite by using a variational technique similar to that of Hashin and Shtrikman (1963). Ponte Castañeda (1996) developed a second-order technique for homogenization of multi-phase materials into a nonlinear homogeneous material, given prior knowledge of the stress concentrations within the composite and an admissible constitutive relation. Many researchers have focused on composites with a viscoplastic matrix and an elastic particulate/inclusion (e.g. see Ponte Castañeda, 2002; Doghri and Friebel, 2005; Dvorak and Srinivas, 1999), as this is more common with epoxy/carbon systems and metal matrix systems such as aluminum/silicon carbide (see Dai et al. (2004)). As discussed by Pindera and Aboudi (1988) the mean-field approach applied to metal-matrix composites does not predict yielding along certain directions in the stress space. Dvorak (2000) has summarized several approaches of different complexity to model inelastic response of multiphase materials.

The inelastic response of the matrix phase is usually considered through the average values of the inelastic strain field either in the entire matrix phase or in the subvolumes into which the matrix phase is partitioned. Methods that employ sub-volume discretization of the unit cell include the generalized method of cells due to Paley and Aboudi (1992). In the transformation field analysis of Dvorak (1992) the strain field is assumed to be piecewise uniform. This approach has been generalized by Chaboche et al. (2001) to better capture the local stress and the inelastic strain fields. Walker et al. (1994) and Fotiu and Nemat-Nasser (1996) have developed techniques that employ more accurate field representations within the repeating unit cell. More recently, Aboudi et al. (2001), Chaboche et al. (2005), Pierard and Doghri (2006), Kachanov and Sevostianov (2005), Liu and Hu (2005), Ohno et al. (2001), Sun and Ju (2004), Pindera et al. (1993) and Wilkinson et al. (2001) have proposed techniques to account for elastoplastic deformations of constituents of a metal-matrix composite. However, these techniques do not generally apply to a system where both the matrix and the particulates experience large plastic deformations.

Here, we seek to determine the effective thermoelastoviscoplastic properties for WHA particulate composites. These composites consist of nearly spherical tungsten (W) particulates, between 30 and 70 μm in diameter, embedded in a nickel–iron (NiFe) matrix. For a random distribution of W particulates in the NiFe matrix the overall response of the composite will be isotropic. Ideally one should analyze a three-dimensional problem and consider particulate size and distribution representative of that used in practical applications. However, we simplify the problem considerably and study plane strain thermomechanical deformations of a WHA. Thus tungsten particulates are circular cylinders rather than spherical particulates. The response of a structure reinforced with unidirectional fibers is not isotropic. However, WHAs are generally modeled as isotropic, and our approximation of studying their plane strain deformations is to determine quickly their effective material properties with reasonable computational resources. We note that Young's modulus for W is very close to that for NiFe, and Poisson's ratio for them has the same value. Thus Young's modulus and Poisson's ratio of the composite can be easily determined from one of the micromechanical models or the rule of mixtures. However, values of their quasistatic yield stresses and material parameters characterizing strain hardening, strain-rate hardening and thermal softening are quite different. Micromechanical models for evaluating effective values of these parameters are non-existent.

We utilize a representative volume element (RVE) indicative of the microstructure of the composite; this RVE is subjected to a variety of thermomechanical deformations in order to find stress–strain curves. These curves are used to estimate strain and strain-rate hardening and thermal softening parameters for the composite. The effects of RVE size, particulate distribution, particulate diameter, and volume fraction of the particulates are considered. Values of the elastic and the thermal parameters are also computed from an analysis of deformations of a RVE so as to compute values of all parameters from numerical tests.

The paper is organized as follows. Equations governing thermomechanical deformations of an isotropic elasto-thermo-viscoplastic material are summarized in Section 2.1. Initial and boundary conditions, and continuity conditions at a particulate/matrix

interface are then stated. Section 2.4 gives a weak formulation of the problem used to develop a computer code for solving numerically the set of coupled nonlinear partial differential equations. The rule of mixtures is described in Section 2.6. Values assigned to thermophysical parameters for tungsten and nickel–iron are tabulated in Section 2.7. The technique developed and the numerical experiments performed to extract values of effective material parameters for the composite from results of deformations of a RVE are given in Section 3. The technique is applied in Section 4 first to ensure that it correctly predicts values of a known homogeneous material and then to ascertain the appropriate size of a RVE, finite element mesh, and particulate size and arrangement. Values of material parameters of a WHA as a function of the volume fraction of constituents are also given in Section 4. These values are then used to compute the response of a WHA employing a RVE and an equivalent homogenized body to simple shearing deformations, plane strain deformations involving loading, unloading and reloading, and axisymmetric deformations. Section 5 describes a semi-inverse technique used earlier by Batra and Kim (1990) for identifying values of material parameters from a known experimental stress–strain curve but it is not used here to find values of effective material parameters. Time histories of the effective plastic strain at a point in each constituent and of the effective plastic strain averaged over each constituent are given in Section 6. The latter are used in the stress–strain relation for each constituent to find a pseudo-effective stress in a constituent. The rule of mixture is applied to these pseudo-effective stresses and volume fractions of constituents to ascertain the effective stress for the composite. Principal findings of the present work are summarized in Section 7 entitled conclusions.

2. Formulation of the problem

2.1. Governing equations

We use rectangular Cartesian coordinates and the referential description of motion to describe transient coupled thermomechanical deformations of an isotropic elasto-thermo-viscoplastic body deformed at a high strain-rate in plane strain tension. Deformations of each constituent and the composite body are governed by the following equations expressing, respectively, the balance of mass, the balance of linear momentum, the balance of moment of momentum, and the balance of internal energy. Except when explicitly mentioned otherwise the indices take values 1 and 2

$$\rho J = \rho_0, \tag{1}$$

$$\rho_0 \dot{v}_i = T_{i\alpha,\alpha}, \tag{2}$$

$$T_{i\alpha} F_{j\alpha} = T_{j\alpha} F_{i\alpha}, \tag{3}$$

$$\rho_0 \dot{e} = -Q_{\alpha,\alpha} + T_{i\alpha} \dot{F}_{i\alpha}. \tag{4}$$

Here, ρ is the present mass density, $J = \det \mathbf{F}$, $F_{i\alpha} = x_{i,\alpha} = \partial x_i / \partial X_\alpha$ the deformation gradient, $\mathbf{x}$ the present position at time t of a material particle located at the place $\mathbf{X}$ in the reference configuration, $\mathbf{T}$ the first Piola–Kirchhoff stress tensor, e the

specific internal energy, $\mathbf{Q}$ the present heat flux measured per unit reference area, $\mathbf{v}$ the velocity of a material particle, a superimposed dot indicates the material time derivative, and a repeated index implies summation over the range of the index. Greek indices refer to coordinates in the reference configuration, and Latin indices to coordinates in the present configuration.

We assume that the strain-rate tensor $\mathbf{D}$ defined by $D_{ij} = (v_{i,j} + v_{j,i})/2$, $v_{i,j} = \partial v_i / \partial x_j$, has the additive decomposition into an elastic part $\mathbf{D}^e$, a plastic part $\mathbf{D}^p$ and a thermal part $\hat{\alpha}\dot{\theta}\mathbf{1}$, viz.,

$$\mathbf{D} = \mathbf{D}^e + \mathbf{D}^p + \hat{\alpha}\dot{\theta}\mathbf{1}, \tag{5}$$

where $\hat{\alpha}$ is the coefficient of thermal expansion, $\mathbf{1}$ is the identity matrix, and θ the temperature rise. Eqs. (1)–(5) are supplemented with the following constitutive relations:

$$\dot{\sigma}_{ij} + \sigma_{ik}W_{kj} - \sigma_{jk}W_{ik} = \frac{E}{1+v}D^e_{ij} + \frac{Ev}{(1+v)(1-2v)}D^e_{kk}\delta_{ij}, \tag{6}$$

$$\dot{e} = c\tau\ddot{\theta} + c\dot{\theta} + \frac{1}{\rho}\sigma_{ij}D^e_{ij}, \tag{7}$$

$$T_{i\alpha} = J\sigma_{ij}(F^{-1})_{\alpha j}, \tag{8}$$

$$q_i = -\kappa\theta_{,i}, \quad Q_\alpha = Jq_i(F^{-1})_{\alpha i}, \tag{9}$$

$$\phi \equiv \frac{\sigma^2_e}{\sigma^2_y} - 1 = 0, \quad \sigma^2_e = \frac{3}{2}\sigma'_{ij}\sigma'_{ij}, \quad i,j = 1,2,3, \tag{10}$$

$$D^p_{ij} = \dot{\lambda}\frac{\partial\phi}{\partial\sigma_{ij}} = \dot{\lambda}\frac{3\sigma'_{ij}}{\sigma^2_y}, \quad \sigma'_{ij} = \sigma_{ij} + p\delta_{ij}, \tag{11}$$

$$p = -(\sigma_{11} + \sigma_{22} + \sigma_{33})/3, \tag{12}$$

$$\dot{\lambda} = \begin{cases} \frac{\sigma_y\dot{\varepsilon}^p_e}{\sigma_{ij}\frac{\partial\phi}{\partial\sigma_{ij}}} & \text{if } \phi = 0 \text{ and } \dot{\phi} \geqslant 0, \\ 0 & \text{when either } \phi < 0 \text{ or } \phi = 0 \text{ and } \dot{\phi} < 0, \end{cases} \tag{13}$$

$$\sigma_y = (A + B(\varepsilon^p_e)^n)\left(1 + C\ln\left(\frac{\dot{\varepsilon}^p_e}{\dot{\varepsilon}_0}\right)\right)\left(1 - \left(\frac{\theta - \theta_r}{\theta_m - \theta_r}\right)^m\right). \tag{14}$$

The left-hand side of Eq. (6) equals the Jaumann derivative of the Cauchy stress tensor $\boldsymbol{\sigma}$, $W_{ij} = (v_{i,j} - v_{j,i})/2$ is the spin tensor, E Young's modulus, v Poisson's ratio, δ_{ij} the Kronecker delta, c the specific heat, τ the thermal relaxation time, and κ the thermal conductivity of the material. Constitutive relation (6) implies that each constituent is being modeled as an isotropic hypoelastic material. Replacing the Jaumann derivative of $\boldsymbol{\sigma}$ by another objective stress rate will change the constitutive description of the material. Eq. (10)$_1$, i.e., $\phi = 0$ describes the von Mises yield surface, p is the hydrostatic pressure, and $\boldsymbol{\sigma}'$ the deviatoric Cauchy stress. Eq. (11)$_1$ is the associated flow rule and $\dot{\lambda}$ is the factor of proportionality defined by Eq. (13); $\dot{\lambda} > 0$ only when the material point is deforming plastically. σ_y is the current yield stress of the material whose dependence upon the effective plastic strain ε^p_e, the effective plastic strain rate $\dot{\varepsilon}^p_e$ and the temperature θ is described by the Johnson–Cook (1983)

relation (14) in which A, B, C, $\dot{\varepsilon}_0$, and m are material parameters, θ_r the room temperature and θ_m the melting temperature of the material. Parameters B and n characterize the strain hardening of the material, C and $\dot{\varepsilon}_0^p$ the strain-rate hardening and the last factor on the right-hand side of Eq. (14) its thermal softening.

Substitution from Eqs. (5) (), (7)–(9) into Eq. (4) gives the following hyperbolic heat equation:

$$\rho_0 c(\tau\ddot{\theta} + \dot{\theta}) = (\kappa\theta_{,\alpha})_{,\alpha} + J\sigma_{ij}D_{ij}^p. \tag{15}$$

The term $J\sigma_{ij}D_{ij}^p$ equals the heating due to plastic working per unit volume in the reference configuration; thus the Taylor–Quinney parameter has been taken as 1. That is, all of the plastic working is assumed to be converted into heating. The form (15) of the hyperbolic heat equation is due to Cattaneo (1958) and Vernotte (1958). The thermal relaxation time τ in it represents the time required to establish a steady state of heat conduction in an element suddenly exposed to heat flux. According to Chester (1963) τ equals $3\kappa/\rho c V_0^2$ where V_0 is the speed of an elastic wave. Thus for a typical steel, $\tau = 1 \times 10^{-12}$ s, and $\tau \simeq 25 \times 10^{-12}$ s for copper. Batra (1975) considered higher-order spatial and temporal gradients of temperature and derived a heat equation that admits finite speeds of thermal waves. However, in such a material either a thermal wave propagates with a finite speed or the linearized problem has a unique solution. Ideally, one will like to have both.

The decision to use the Johnson–Cook relation (14) here is based on the availability of values of thermomechanical parameters for tungsten and nickel–iron.

Numerical experiments to evaluate values of the particulate composite are performed at a uniform temperature. Thus the precise value of the Taylor–Quinney parameter is Eq. (15) plays very little role.

2.2. Initial and boundary conditions

The body is initially taken to be at rest, at a uniform temperature and has no initial stress. Thus,

$$\mathbf{x}(\mathbf{X}, 0) = \mathbf{X}, \quad \mathbf{v}(\mathbf{X}, 0) = \mathbf{0}, \quad \theta(\mathbf{X}, 0) = \theta_0, \quad \dot{\theta}(\mathbf{X}, 0) = 0,$$
$$\rho(\mathbf{X}, 0) = \rho_0(\mathbf{X}), \quad \boldsymbol{\sigma}(\mathbf{X}, 0) = \mathbf{0}, \quad \varepsilon_e^p(\mathbf{X}, 0) = 0, \quad \mathbf{X} \in \Omega, \tag{16}$$

where Ω is the region occupied by the body in the reference configuration.

A square RVE with side length H is subjected to a "constant area plane strain tension test". The upper surface of the body is given a constant velocity v_0 in the X_2-direction after a short ramp time of 1 μs. The lower surface of the body is held fixed in the X_2-direction and is allowed to slide smoothly in the X_1-direction. The lateral smooth surfaces are prescribed a velocity in the X_1-direction such that the area of the rectangle remains a constant H^2, as shown in Fig. 1(a). This choice of deformation is somewhat arbitrary; however, it does guarantee that the shape of the boundary remains well-defined, despite the inhomogeneous material of the RVE. Also, the area-preserving deformation of the RVE is consistent with the incompressibility assumption made in the flow rule associated with the von Mises yield surface,
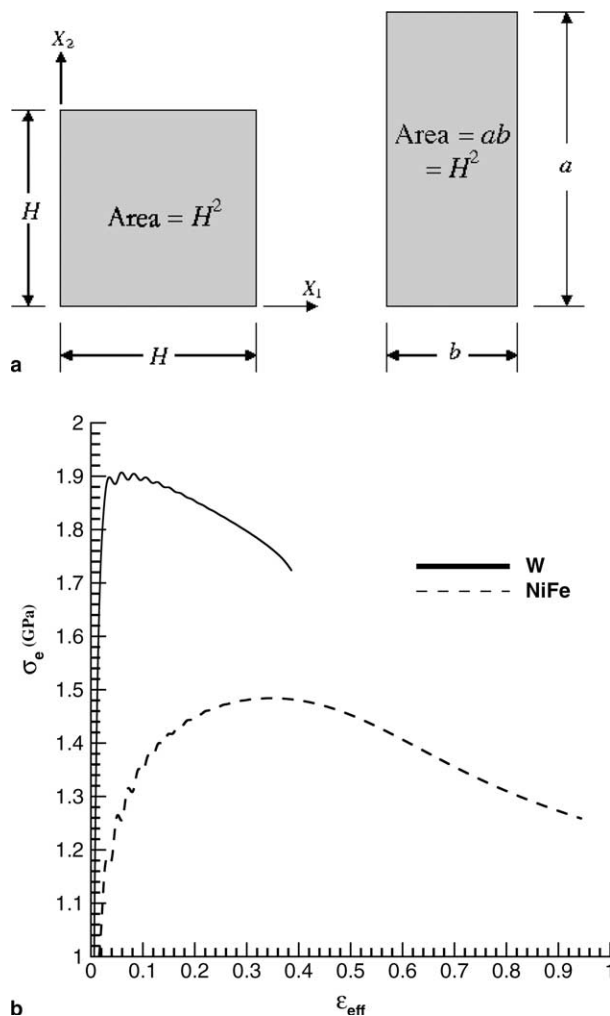
Fig. 1. (a) Sketch of constant-area plane-strain deformation used for finding effective properties of a composite. (b) Effective stress versus effective plastic strain curve for plane strain extensional deformations of tungsten and nickel–iron.

making this deformation admissible for large plastic deformations. All bounding surfaces of the RVE are taken to be thermally insulated.

2.3. Interface conditions

It is assumed that, during the entire deformation process, the W particulates are both mechanically and thermally perfectly bonded to the NiFe matrix. Thus

$$[\mathbf{u}] = \mathbf{0}, \quad [\theta] = 0, \quad [T_{i\alpha}N_\alpha] = 0, \quad [Q_\alpha N_\alpha] = 0 \quad \text{on } \Gamma, \tag{17}$$

where $\mathbf{N}$ is an outward unit normal, in the reference configuration, to the interface Γ between a particulate and the matrix, $\mathbf{u}$ is the displacement of a point, and the square bracket indicates the jump of a quantity across the interface Γ between a particulate and the matrix.

2.4. Semi-discrete formulation of the problem

Eqs. (6), (8) and (3) imply that the balance of moment of momentum (3) is identically satisfied. The present mass density can be computed from Eq. (1) if the deformation gradient is known. Thus, the dependent variables to be solved for are $\mathbf{x}$ and θ and the independent variables are $\mathbf{X}$ and t. Eqs. (2) and (15) are second-order coupled non-linear hyperbolic partial differential equations for $\mathbf{x}$ and θ. These cannot be written explicitly in terms of $\mathbf{x}$ and θ since $\mathbf{T}$ is given by (8) and $\dot{\boldsymbol{\sigma}}$ by (6) which involves $\mathbf{D}^{\mathrm{p}}$ and θ because of Eq. (5). In order to solve the problem numerically by the FE method, we first derive its weak or variational formulation.

Let $\mathbf{w}(\mathbf{X})$ be a smooth function that is an analog of virtual velocity, and it vanish at the boundary points wherever $\mathbf{v}$ is prescribed. We take the inner product of Eq. (2) with $\mathbf{w}$, integrate the resulting equation over the region Ω occupied by the body in the reference configuration, and use the divergence theorem to arrive at

$$\int_{\Omega} \rho_0 \dot{v}_i w_i \, \mathrm{d}\Omega = - \int_{\Omega} w_{i,\alpha} T_{i\alpha} \, \mathrm{d}\Omega + \int_{\Gamma_t} w_i \bar{t}_i \, \mathrm{d}\Gamma, \tag{18}$$

where $\bar{t}_i$ is the surface traction prescribed at boundary points. For the present problem, $\bar{\mathbf{t}} = \mathbf{0}$. Let $\psi_1, \psi_2, \ldots, \psi_n$ be the FE basis functions defined on Ω. We write

$$v_i = \sum_{A=1}^{\text{nodes}} \psi_A(\mathbf{X}) \tilde{v}_{Ai}(t), \quad w_i = \sum_{A=1}^{\text{nodes}} \psi_A(\mathbf{X}) c_{Ai}. \tag{19}$$

Here, $\tilde{\mathbf{v}}$ is the vector of velocities of nodes, and c_{Ai}'s are constants. Substituting for $\mathbf{v}$ and $\mathbf{w}$ from Eq. (19) into Eq. (18) and exploiting the fact that the resulting equation must hold for all choices of $\mathbf{c}$'s (e.g., see Hughes, 1987) we get

$$\mathbf{M}\dot{\tilde{\mathbf{v}}} = -\mathbf{F}^{\text{int}} + \mathbf{F}^{\text{ext}},$$
$$M_{AB} = \int_{\Omega} \rho_0 \psi_A \psi_B \, \mathrm{d}\Omega, \, F_{Ai}^{\text{int}} = \int_{\Omega} \psi_{A,\alpha} T_{i\alpha} \, \mathrm{d}\Omega, \, F_{Ai}^{\text{ext}} = \int_{\Gamma_t} \psi_A \bar{t}_i \, \mathrm{d}\Gamma. \tag{20}$$

In order to derive a weak form of Eq. (15) we first introduce an auxiliary variable

$$\xi = \dot{\theta}, \tag{21}$$

and adopt the same procedure as that used to derive Eq. (20) with the following result:

$$\dot{\boldsymbol{\theta}} = \tilde{\boldsymbol{\xi}},$$
$$\tau \mathbf{H}\dot{\tilde{\boldsymbol{\xi}}} + \mathbf{H}\tilde{\boldsymbol{\xi}} = \mathbf{F}^{\theta} + \tilde{\mathbf{Q}}, \tag{22}$$

where

$$H_{AB} = \int_{\Omega} \rho_0 c \psi_A \psi_B \, d\Omega, \quad F_A^{\theta} = \int_{\Omega} \kappa \theta_{,\alpha} \psi_{A,\alpha} \, d\Omega, \quad Q_A = \int_{\Omega} \psi_A J \text{tr}(\boldsymbol{\sigma} \mathbf{D}^{\mathrm{p}}) \, d\Omega. \tag{23}$$

Note that the natural boundary condition of zero heat flux on all bounding surfaces has been embedded in Eq. (22). Solving Eq. (14) for $\dot{\varepsilon}_{\mathrm{e}}^{\mathrm{p}}$ in terms of σ_{y}, $\varepsilon_{\mathrm{e}}^{\mathrm{p}}$ and θ we get

$$\dot{\varepsilon}_{\mathrm{e}}^{\mathrm{p}} = \dot{\varepsilon}_0 \exp\left[\frac{\sigma_{\mathrm{y}}}{(A + B(\varepsilon_{\mathrm{e}}^{\mathrm{p}})^n)(1 - \theta_*^m)} - 1 \right], \tag{24}$$
$$\theta_* = (\theta - \theta_{\mathrm{r}})/(\theta_{\mathrm{m}} - \theta_{\mathrm{r}}).$$

Similar to the approximation $(19)_1$ for the velocity field we assume that

$$\dot{\varepsilon}_{\mathrm{e}}^{\mathrm{p}}(\mathbf{X}, t) = \sum_{A=1}^{\text{nodes}} \psi_A(\mathbf{X}) \dot{\varepsilon}_{\mathrm{e}A}^{\mathrm{p}}(t), \quad \tilde{\omega}(\mathbf{X}) = \sum_{A=1}^{\text{nodes}} \psi_A(\mathbf{X}) c_A, \tag{25}$$

Multiplication of both sides of Eq. $(24)_1$ with the test function $\tilde{\omega}$, integration of the resulting equation over the domain Ω, substitution in it for $\dot{\varepsilon}_{\mathrm{e}}^{\mathrm{p}}$ and $\tilde{\omega}$ from Eq. (25) and exploiting the arbitrariness of constants $c_1, c_2, \ldots$, we obtain

$$\tilde{\mathbf{M}} \dot{\boldsymbol{\varepsilon}}_{\mathrm{p}}^{\mathrm{e}} = \tilde{\mathbf{F}}, \tag{26}$$

where

$$\tilde{M}_{AB} = \int_{\Omega} \psi_A \psi_B \, d\Omega, \quad \tilde{F}_A = \dot{\varepsilon}_0 \int_{\Omega} \exp\left[\frac{\sigma_{\mathrm{y}}}{(A + B(\varepsilon_{\mathrm{e}}^{\mathrm{p}})^n)(1 - \theta_*^m)} - 1 \right] \psi_A \, d\Omega. \tag{27}$$

We note that the integrand in the integral on the right-hand side of Eq. (27) is zero at the integration or the quadrature point that is either deforming elastically or is unloading.

The weak form of

$$\dot{\mathbf{x}} = \mathbf{v}(\mathbf{X}, t) \tag{28}$$

is also derived in the same way as that for $\dot{\varepsilon}_{\mathrm{e}}^{\mathrm{p}}$ given by Eq. (24). We thus get coupled nonlinear ordinary differential equations

$$\dot{\mathbf{d}} = \mathbf{F}, \tag{29}$$

where $\mathbf{d}$ is the vector of unknowns and $\mathbf{F}$ is the force vector that depends upon time t and $\mathbf{d}(t)$. The unknowns at a node are $\{x_1, x_2, v_1, v_2, \theta, \xi, \varepsilon_{\mathrm{e}}^{\mathrm{p}}\}$.

The constitutive relation (6) is integrated at the quadrature points in an element. Thus for a FE mesh comprised of 4-node quadrilateral elements with 2×2 integration rule, the total number of unknowns equals 7 (number of nodes) + 4 (number of elements).

2.5. Verification of the computer code

A computer code based on the semi-discrete formulation has been developed using 4-node quadrilateral elements. Spatial integration is accomplished over each element using 2×2 Gaussian quadrature rule. Spatial variation in material properties is

considered in the integration by using local values at each quadrature point. Natural boundary conditions of null tangential tractions are already included in Eq. (29). Suitable modifications to the equations are made to enforce velocity components prescribed at boundary points. Eqs. (29) and (6) evaluated at the Gauss integration points are then integrated using the Livermore solver for ordinary differential equations (LSODE); parameter MF in LSODE is set equal to 10, which implies an Adams–Moulton method. The absolute and relative tolerances in LSODE are set to 10^{-7}. LSODE adaptively adjusts the timestep in order to compute the solution to within the desired accuracy, and is freely available on the internet in both Fortran and C++ variants.

The computer code was validated by comparing computed results for several problems with their published analytical and/or numerical solutions and was also validated by the method of ficticious body forces (sometimes also called the method of manufactured solutions). In this method, body forces and sources of internal energy density are found for any assumed deformation and temperature fields so that the governing equations are satisfied. These fields are input into the code. The computed solution should match the presumed analytical solution to a high degree of accuracy; see the material following Eq. (30) in Batra and Liang's (1997) paper for an example. Furthermore, the solution for finite plastic deformations of a homogeneous body with inhomogeneous initial and boundary conditions coincided with Batra and Lear's (2005) solution obtained with triangular elements.

2.6. Rule of mixtures

According to this rule, the value P of a material parameter for a mixture comprised of two constituents with volume fractions V_1^f and V_2^f and values P_1 and P_2 of the material parameter is given by

$$P = V_1^f P_1 + V_2^f P_2 = (1 - V_2^f)P_1 + V_2^f P_2. \tag{30}$$

It gives exact values of the mass density and the heat capacity and often gives an upper bound for values of other elastic parameters for the composite.

2.7. Values of material parameters

Values of thermophysical parameters for tungsten (W) and nickel–iron (NiFe) are listed in Tables 1 and 2.

Thus the acoustic impedances, $\sqrt{E\rho}$, of W and NiFe equal 87.86×10^6 and 48.44×10^6 kg/(m^2 s), respectively, and differ by a factor of 1.8. The bar wave speeds, $\sqrt{(E/\rho)}$, in W and NiFe are 4552 and 5265 m/s and differ by a factor of 0.86.

Fig. 1(b) shows the effective stress versus the effective plastic strain curve for homogeneous W and NiFe bodies deformed in overall adiabatic plane strain tension at a nominal axial strain rate of 5000/s with traction free lateral edges. It is clear that the yield stress for W is considerably higher than that for NiFe, the peak value of the effective stress in W is reached at a considerably lower value of the effective plastic strain than that in NiFe and the thermal softening in W is significantly higher than that in NiFe.

Table 1
Values of elastic and thermal parameters for W, NiFe and steel

Material	E (GPa)	v	ρ (kg/m³)	κ (W/m K)	$\hat{\alpha}$ (×10⁻⁶/K)	c (J/kg K)
W	400	0.29	19,300	160	5.3	138
NiFe	255	0.29	9200	100	15.0	382
Steel	210	0.27	7840	38	12.6	477

Table 2
Values of viscoplastic parameters for W, NiFe and steel

Material	A (MPa)	B (MPa)	n	C	$\dot{\varepsilon}_0$ (1/s)	θ_m (K)	m
W	730	562	0.0751	0.0290	1.4×10^{-13}	1700	1
NiFe	150	546	0.2080	0.0838	6.7×10^{-14}	1225	1
Steel	1100	510	0.26	0.04	7×10^{-14}	1793	1

Whereas values of E, v, B and m for the two constituents are nearly the same, those of other thermal and viscoplastic parameters are quite different.

3. Determination of values of effective material parameters

Determination of elastic and viscoplastic parameters from a series of thermomechanical deformations of an RVE is a non-trivial task. In a macro-scale analysis, the RVE itself is small enough to be considered a material point; that is, one could regard it having uniform material properties, stresses and strains. Thus, an effective stress and an effective strain tensor for the deformation of the RVE should be defined.

For the constant-area plane-strain biaxial tension deformation described in Section 2, we define the Cauchy stress tensor as follows. Recall that the length in the x_3-direction equals one, and it stays unchanged during plane strain deformations in the x_1x_2-plane, σ_{22} equals the total normal load divided by the present length of the top or the bottom edges (e.g., see Fig. 1(a)), σ_{11} is the normal load on a lateral edge divided by its present length, σ_{12} is the tangential load on an edge divided by its present length (which is, not surprisingly, nearly zero for this deformation), and σ_{33} is the total load in the x_3-direction divided by the current area perpendicular to the x_3-axis.

Large deformations require the definition of a suitable strain tensor. The deformation described in Section 2 results in the initial square being deformed into a rectangle. For a homogeneous material, this would be a homogeneous deformation; so, we assume that $F_{11} = H/a$, $F_{22} = a/H$, and $F_{33} = 1$, where a is the current x_2-coordinate of the top surface (as shown in Fig. 1), and the Almansi–Hamel strain tensor is then defined as:

$$\varepsilon_{ij} = (\delta_{ij} - B_{ij}^{-1})/2. \tag{31}$$

Here, $B_{ij} = F_{i\alpha}F_{j\alpha}$ is the left Cauchy-Green tensor. The von Mises effective stress can be computed from Eq. (10)$_2$, and the effective strain from $\varepsilon_e = \sqrt{\frac{3}{2}\varepsilon_{ij}\varepsilon_{ij}}$. Initial numerical analyses are conducted with the heat generated during plastic working set equal to zero (i.e., neglected) resulting in $\dot\theta = 0$. Therefore, the thermal and the mechanical properties are divorced from each other and are treated separately.

3.1. Mass density and specific heat

The rule of mixtures (30) gives exact values of the effective mass density and the effective heat capacity of the composite. The effective specific heat can be computed from the latter.

3.2. Elastic parameters

Determination of Young's modulus and Poisson's ratio is relatively simple using the stress and the strain tensors defined in the previous section. For metals, deformations in the elastic regime are relatively small (strains $\lesssim 0.3\%$). For infinitesimal deformations, $\sigma_{ik}\,w_{kj}$ in Eq. (6) is negligible as compared to other terms, and the resulting equation is integrated to obtain Hooke's law written as Eqs. (32)–(34). Quasistatic elastic deformations can be produced by assigning a very small value to the mass density ρ_0 and a rather large value to the quasistatic yield stress A. For plane strain deformations of an isotropic linear elastic material:

$$\varepsilon_{11} = \frac{1}{E}[\sigma_{11} - v(\sigma_{22} + \sigma_{33})], \tag{32}$$

$$\varepsilon_{22} = \frac{1}{E}[\sigma_{22} - v(\sigma_{11} + \sigma_{33})], \tag{33}$$

$$\varepsilon_{33} = 0 = \frac{1}{E}[\sigma_{33} - v(\sigma_{11} + \sigma_{22})]. \tag{34}$$

With results from a constant-area plane strain tension test, Eq. (34) can be solved for Poisson's ratio, v. Using this result, one can compute Young's modulus from either Eq. (32) or Eq. (33) with the other equation offering a check on the isotropy of the particulate arrangement.

3.3. Quasistatic yield stress, and strain and strain-rate hardening parameters

Determination of the quasi-static yield stress A and the strain hardening parameters B and n in the Johnson–Cook relation is difficult from an examination of an effective stress versus effective strain curve. For a given material, there are several different combinations of values of A, B and n that produce essentially the same stress–strain curve. The onset of yielding (corresponding to an effective stress of A in a quasi-static test) is not readily apparent when examining the stress–strain curve or its derivative because the strain-rate hardening term in the Johnson–Cook relation prevents a noticeable change in the slope of the curve at the yield strain; e.g., see Fig. 1(b). Fig. 2 compares values of A computed from the rule of mixtures with those
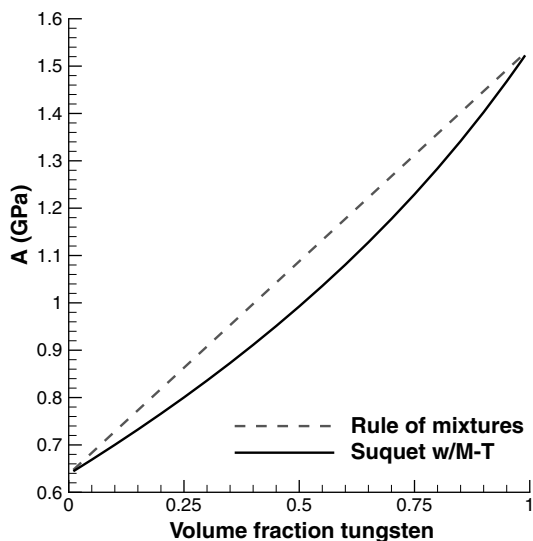
Fig. 2. Comparison of yield stress estimates from the rule of mixtures and Suquet's method using the Mori–Tanaka estimate for the shear modulus.

obtained from Suquet's (1993) relation, with the effective shear modulus computed from the Mori and Tanaka (1973) relation and values of A for W and NiFe taken from Table 2 given in Section 2.7. We have chosen to estimate A of the composite from the rule of mixtures.

Conducting a plane-strain tension test (as described in Section 2) at an effective strain-rate close to the reference strain rate $\dot{\varepsilon}_0$ then allows the determination of the yield strain from the estimated value of A; the effective plastic strain ε_e^p is then defined as the total effective strain minus the effective strain at yield. The approximate value of the effective plastic strain ε_e^p so obtained is reasonably good since the effective plastic strain at yield is miniscule. Plotting $\log(\sigma_y - A)$ versus $\log(\varepsilon_e^p)$ allows the determination of B and n from a simple linear least squares fit; n equals the slope of the line and $\log B$ the y-intercept. Through numerical tests it was shown that the use of a different technique for determining A, such as the method proposed by Suquet (1993), produces quantitatively different values for B and n, but the resulting stress–strain curve is effectively the same.

The effective strain-rate hardening coefficient C can be determined by examining two tests performed at different effective strain-rates on the same RVE. We have taken the reference strain-rate $\dot{\varepsilon}_0$ to be the same for the two constituents and the composite. Given the stress–strain curve for the two different tests, the value of C can be calculated from

$$C = \frac{1 - \frac{\sigma_{y1}}{\sigma_{y2}}}{\frac{\sigma_{y1}}{\sigma_{y2}} \ln\left(\frac{\dot{\varepsilon}_2}{\dot{\varepsilon}_0}\right) - \ln\left(\frac{\dot{\varepsilon}_1}{\dot{\varepsilon}_0}\right)}. \tag{35}$$

Here, σ_{y1} and σ_{y2} are the flow stresses at the same effective plastic strain during deformations at nominal strain-rates of $\dot{\varepsilon}_1$ and $\dot{\varepsilon}_2$, respectively.

3.4. Thermal softening parameters

Thermal softening in the Johnson–Cook relation is governed by θ_m, the "melting" temperature of the material, and m, a thermal exponent. Note that as the temperature approaches θ_m, the yield stress of the material approaches zero. Here, we assume that the thermal exponent m equals 1 for both constituents and the composite, as it is nearly equal to 1 for most materials.

To determine the effective melting temperature of the composite, we conduct plane strain tension tests at different uniform temperatures. As in the other tests, plastic working is neglected; initial attempts at relaxing this assumption resulted in transient, non-constant temperature fields in the RVE which were dependent on the effective strain-rate of the test, making it difficult to assign an effective temperature to the RVE. Given the uniform temperature, the ratio of stresses at a given effective plastic strain for two tests with different temperatures allows one to simply determine the effective melting temperature for the composite from

$$\theta_m = \frac{\frac{\sigma_{y1}}{\sigma_{y2}}\theta_2 + \theta_1}{1 - \frac{\sigma_{y1}}{\sigma_{y2}}}. \tag{36}$$

Here, σ_{y1} and σ_{y2} are the flow stresses at the same effective plastic strain strain during tests at temperatures of θ_1 and θ_2, respectively.

It is important to note that the "melting temperature" of the composite governs its thermal softening, but has no physical significance. The actual melting temperature of the composite would equal the lowest of the melting temperatures of its constituents.

3.5. Thermal conductivity

The effective thermal conductivity of the composite is determined by applying a constant temperature differential across two opposite edges of the RVE. The average heat flux on those edges is divided by the applied temperature gradient, giving an effective thermal conductivity. Ideally, one would have a microstructure that gives the same thermal conductivity in the X_1- and the X_2-directions. In practice, this is difficult. The average of the computed thermal conductivities in the X_1- and the X_2-directions is taken as the effective thermal conductivity.

3.6. Coefficient of thermal expansion

The effective coefficient of thermal expansion of the composite is computed by constraining all edges of the RVE from moving in the normal directions (as well as the plane strain constraint) and applying a uniform temperature rise over the entire RVE. Given that the resulting stresses are significantly below the yield stress, we set $\mathbf{D}^p = \mathbf{0}$ in Eq. (5), take the trace of Eq. (6), integrate the resulting equations with

respect to time and obtain Eq. (37). The effective coefficient of thermal expansion is computed from:

$$\hat{\alpha} = \frac{-\sigma_{kk}}{9K\Delta T}. \tag{37}$$

Here, K is the *effective* bulk modulus of the material and ΔT is the temperature rise; K is computed from E and v. Note that it is assumed that the coefficient of thermal expansion is a scalar, tacitly assuming an isotropic material.

4. Application of the method of Section 3

4.1. Verification

In an attempt to verify the plausibility and the accuracy of the methods described above, we examined mechanical deformations of a pure tungsten specimen of square cross-section of length $H = 0.25$ mm. The reference strain-rates listed in Table 2 are far too slow to allow numerical tests without significant strain-rate effects, so the reference strain-rate needs to be altered. For two reference strain-rates of $\dot{\varepsilon}_0$ and $\dot{\varepsilon}_1$, the Johnson–Cook viscoplastic relation (14), without thermal effects, gives

$$\sigma_y = \begin{cases} (A + B(\varepsilon_e^p)^n)\left(1 + C\ln\left(\frac{\dot{\varepsilon}_e^p}{\dot{\varepsilon}_0}\right)\right), \\ (A + B(\varepsilon_e^p)^n)\left(1 + C\ln\left(\frac{\dot{\varepsilon}_e^p}{\dot{\varepsilon}_1}\frac{\dot{\varepsilon}_1}{\dot{\varepsilon}_0}\right)\right), \\ (A + B(\varepsilon_e^p)^n)\left(\left(1 + C\ln\left(\frac{\dot{\varepsilon}_e^p}{\dot{\varepsilon}_1}\right)\right)\left(1 + C\ln\left(\frac{\dot{\varepsilon}_1}{\dot{\varepsilon}_0}\right)\right) - C^2\ln\left(\frac{\dot{\varepsilon}_e^p}{\dot{\varepsilon}_1}\right)\ln\left(\frac{\dot{\varepsilon}_1}{\dot{\varepsilon}_0}\right)\right). \end{cases} \tag{38}$$

Assuming that $C \ll 1$, neglecting the term containing C^2 allows A and B to be computed at the new reference strain-rate:

$$A^* = A\left(1 + C\ln\left(\frac{\dot{\varepsilon}_1}{\dot{\varepsilon}_0}\right)\right), \quad B^* = B\left(1 + C\ln\left(\frac{\dot{\varepsilon}_1}{\dot{\varepsilon}_0}\right)\right). \tag{39}$$

This modification to the material parameters produces a slight error (due to the omission of the C^2 term); however, this error is of the order of 1–2%, far lower than the accuracy level of the material parameters themselves. The modified values A^* and B^* of A and B are listed in Table 3.

With the modified values of material parameters, the pure tungsten RVE was subjected to numerical tests with nominal axial strain-rates of 2500, 5000, 25,000, and 50,000/s, and additional 50,000/s tests were conducted at temperature rises of 100, 200, 500, and 1000 K. Furthermore, uniform FE meshes of 40×40, 60×60, and 80×80 elements were used and they gave identical results for the pure tungsten sample. Using the data from these tests, the effective material parameters for tungsten were computed using the techniques described above; the results are listed in Table 4, along with the percent error from the input values.

Note that the quasi-static yield stress A^* was assumed to be 1536.9 MPa, which was the input value. The accuracy of the proposed method is excellent, producing

Table 3
Modified values A^* and B^* of A and B for a reference strain-rate of 5000/s

Material	A^* (MPa)	B^* (MPa)
W	1536.9	1183.2
NiFe	638.4	2323.6

Table 4
Values obtained from the procedure of Section 3 for pure tungsten

	E (GPa)	v	B^* (MPa)	n	C	θ_m (K)	κ (W/m K)	$\hat{\alpha}$ (10^{-6}/K)
Homog. values	405.94	0.2907	1189.4	0.07813	0.02877	1708	160.0	5.27
% Error	1.49	0.24	0.52	4.03	1.03	0.47	∼0	0.57

less than 4% error for values of all parameters. Use of different strain-rate and temperature tests resulted in slight differences in the computed values of C and θ_m; it was found that using very different strain-rates and a large temperature rise produced more accurate results.

4.2. Representative volume element size

The appropriate size for the RVE is dependent on the microstructure of the material in question. Typical WHAs have W particulates with diameters of ∼50 μm arranged randomly, such that the bulk material is isotropic. An RVE must capture a sufficient number of particulates to give an accurate volume fraction of material and give a near isotropic response.

In order to investigate this effect, four RVEs were created with side lengths of $H = 0.15$, 0.25, 0.35, and 0.50 mm. The FE mesh density was kept constant, with each element measuring 5 μm × 5 μm. Each RVE consists of 50 μm diameter W particulates distributed randomly to give a volume fraction of tungsten equal to 50%. Each of the RVEs was subjected to a plane-strain tension test and then re-tested after a 90° rotation, to insure that the distribution gave nearly isotropic response. Shown in Fig. 3 are the four RVEs and the deviations in effective stress versus effective strain curves for three of them from the fourth one; the deviations in Fig. 3 are normalized with respect to the 0.25 mm RVE's result. All four of the curves agree pointwise to within 1%. The 0.25 mm × 0.25 mm RVE was chosen for the remainder of the analyses, and the effective stress versus the effective strain curve obtained from it is referred to as the standard stress strain curve. One reason for this choice is that a 50 μm diameter circle could be meshed better for this RVE than for the RVE with $H = 0.35$ and 0.50 mm.

4.3. Finite element mesh density

To test the effects of the mesh density on the homogenization results, a 0.25 mm × 0.25 mm RVE consisting of 50% volume fraction of 50 μm diameter W
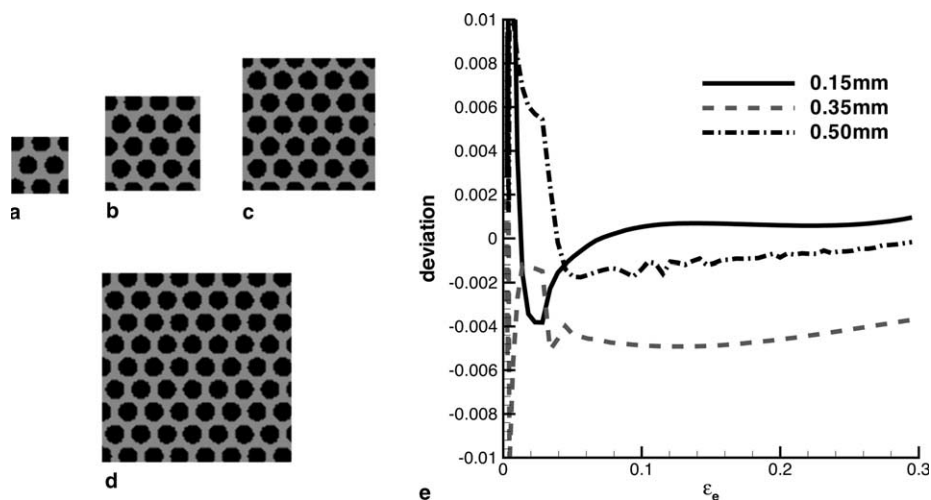
Fig. 3. 50% volume fraction tungsten RVEs with $H =$ (a) 0.15 mm, (b) 0.25 mm, (c) 0.35 mm, and (d) 0.50 mm, and (e) the deviation in the effective stress versus effective strain curve for $H = 0.15$ mm, 0.35 mm, and 0.50 mm from that for $H = 0.25$ mm.

particulates was tested with four different uniform meshes: 40×40, 50×50, 60×60 and 80×80 elements. Fig. 4 shows the RVE and the deviations in the effective stress value for the other three meshes from that for the standard 50×50 mesh. Note that the mesh density does not influence much the computed effective stress versus effective strain results. The 50×50 mesh was chosen for the remainder of the analyses.

4.4. Particulate arrangement

The arrangement of particulates in the RVE could possibly have an effect on the values of the effective parameters. Most WHAs exhibit isotropic behavior, so the arrangement of the particulates must be such that the overall response is independent of direction. To examine this effect, four RVEs with 50% volume fraction of 50 μm diameter W particulates were tested; the first with particulates centered on the vertices of equilateral triangles and the remaining three with different random dispersions of particulates. The deviations of stress–strain curves for these three cases are shown in Fig. 5(a), with the reference curve taken to be that for the ordered arrangement. No effect of particulate arrangement is seen in the overall stress–strain behavior since the maximum deviation is only 0.9%.

4.5. Particulate size

Fig. 5(b) shows the deviation in the stress–strain curves from the testing of three RVEs with 50% volume fraction of W particulates, each test with a different diameter of particulate: 30, 50 and 70 μm. The reference curve was taken to be that for the
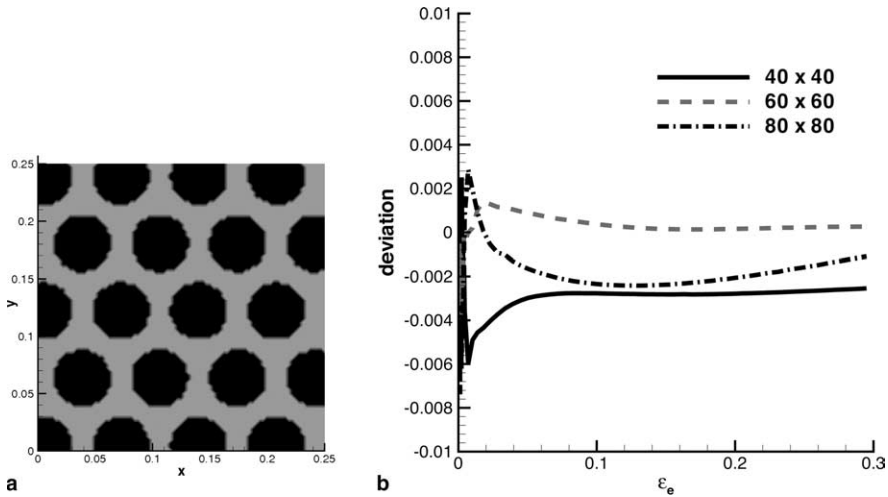
Fig. 4. Finite element mesh density test: (a) 0.25 mm square 50% volume fraction tungsten RVE, (b) the deviations in the stress–strain curves for the 40×40, 60×60, and 80×80 FE meshes from that for the 50×50 mesh.

50 μm particulates. One can see no discernible effect of particulate size from this analysis as the maximum deviation is only 1%.

Thus from results of Figs. 5(a) and (b) one can conclude that any reasonable arrangement of particulates of diameters between 30 and 70 μm will give the same effective stress versus effective strain curve.

4.6. Effective values of parameters as a function of the volume fraction of constituents

Of primary interest to material designers and engineers is the effect of the volume fraction of the particulate on the effective material parameters. Results from Sections 4.1 and 4.2 give an indication of the appropriate RVE size and the FE mesh to study the problem. Sections 4.3 and 4.4 demonstrate that the particulate size and distribution have little effect on the response of the RVE. With these guidelines, a 0.25×0.25 mm RVE meshed with 2500 uniform square elements is studied, using 50 μm diameter particulates centered on the vertices of equilateral triangles. The distance between the particulates is adjusted to give volume fractions between 50% and 80%. Less than 50% volume fraction is of little interest to designers; greater than 80% volume fraction is difficult to achieve with circular particulates. Each RVE was subjected to plane-strain tension tests at nominal axial strain-rates of 5000 and 50,000/s. Additionally, the RVE was tested at 50,000/s with temperature rises of 200 and 500 K.

4.6.1. Elastic parameters

Fig. 6 shows Young's modulus as a function of the volume fraction of W. Values obtained from the rule of mixtures and the Mori–Tanaka method are also plotted as
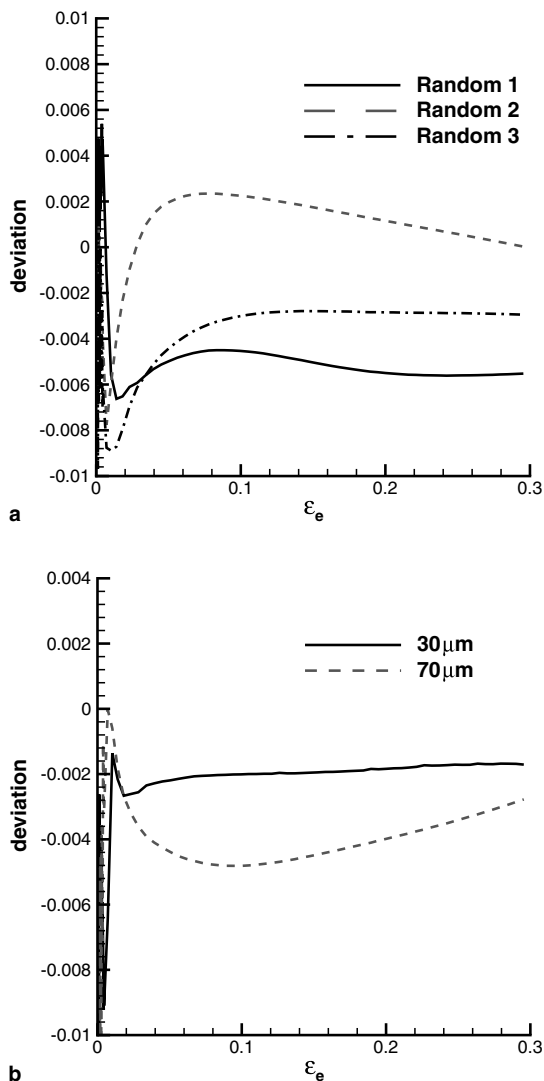
Fig. 5. (a) Deviations in the stress–strain curves from the ordered particulate arrangement for three different random distributions of 50 μm diameter particulates. (b) Deviations in the stress–strain curves from the 50 μm diameter particulate distribution for the 30 and 70 μm diameter particulate distributions.

a reference. The Mori–Tanaka estimate, as shown by Weng (1984), assumes randomly distributed spherical particulates; this plane-strain analysis assumes particulates to be circular cylinders. Despite the non-isotropic arrangement (if one considers the x_3-direction), the homogenized values are quite reasonable. The Poisson's ratio of the composite matched the Poisson's ratio of the constituents within 1% for all volume fractions; it is to be expected since Poisson's ratios of the two constituents are the same.
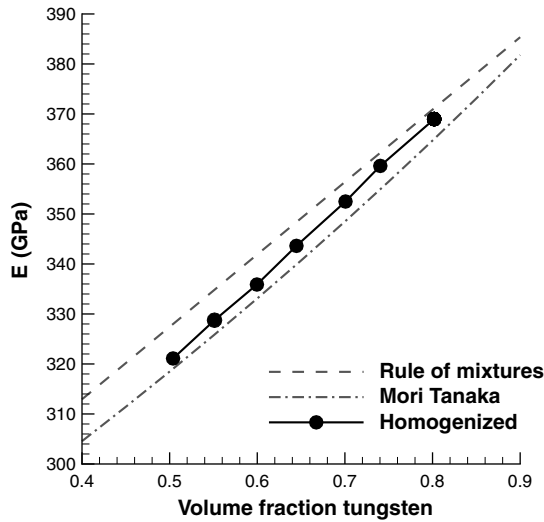
Fig. 6. Effective Young's modulus as a function of volume fraction of tungsten particulates.

4.6.2. Strain hardening parameters

The variation of B^* and n with the volume fraction of W is shown in Figs. 7(a) and (b), respectively. The proposed procedure predicts slightly higher values for B^* and n than the rule of mixtures, but the slope is nearly the same as that of the curve obtained from the rule of mixtures.

4.6.3. Strain-rate hardening parameters

The strain-rate hardening coefficient C was determined for each of the volume fractions at effective plastic strains of 5–30%. Fig. 8(a) shows the value of C at 5% effective plastic strain for each of the volume fractions; results are similar to those obtained from the rule of mixtures. It is important to note that the value of C is different over the range of strains studied. Fig. 8(b) shows C as a function of the effective strain ε_e for each of the tested volume fractions.

One possible explanation for the variation of C with ε_e is the interaction between the particulates and the matrix. As should be evident from the plot of Fig. 1(b) NiFe is much softer than W, so it is deformed more severely in the beginning. Also, it exhibits more strain-rate hardening; so, the initial strain-rate hardening value for the composite is maximum. As the strain increases, more of the W is deformed plastically, lowering the overall strain-rate hardening. This effect is amplified by our choice of a constant value for B^* and n (dictated by the linear curve fit); realistically, B^* and n are also functions of strain. This variation with respect to strain depends upon the microstructure of the material and is difficult to quantify. The situation is somewhat similar to that of a piezocomposite which exhibits pyroelectric effect even if none of the constituents is pyroelectric. Here, C is independent of ε_e for the two constituents but not for the composite.
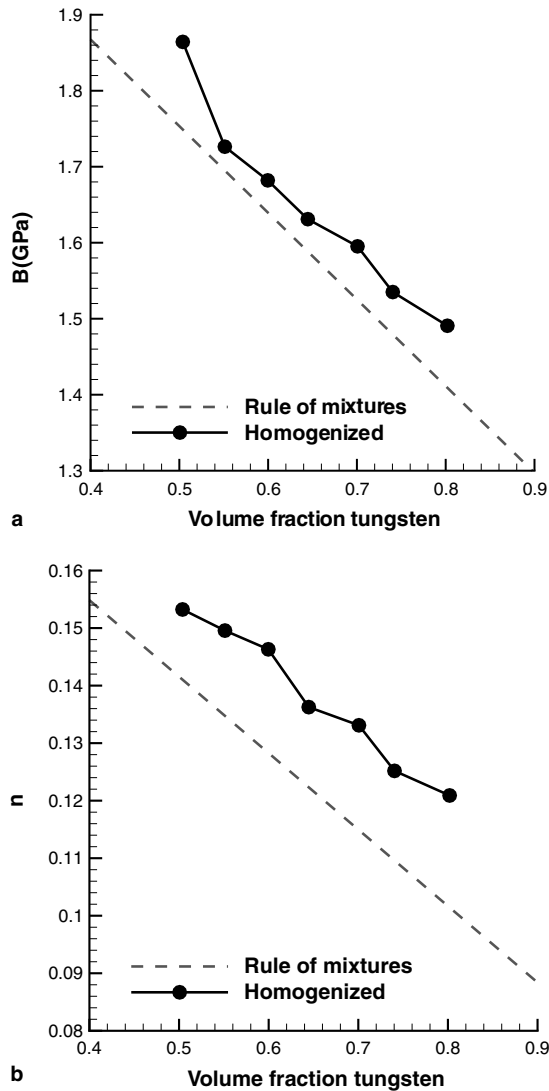
Fig. 7. (a) Strain hardening coefficient B^* as a function of volume fraction of tungsten particulates. (b) Strain hardening exponent n as a function of volume fraction of tungsten particulates.

4.6.4. Thermal softening

Fig. 9(a) shows the melting temperature as a function of the volume fraction of W particulates. The values indicated as $\Delta\theta = +200$ and $+500$ K are obtained by comparing the plane strain tension test at the reference temperature to tests with a temperature rise of 200 and 500 K, respectively. Note that there is a small difference between the two lines. Fig. 9(b) shows the variation in the computed melting
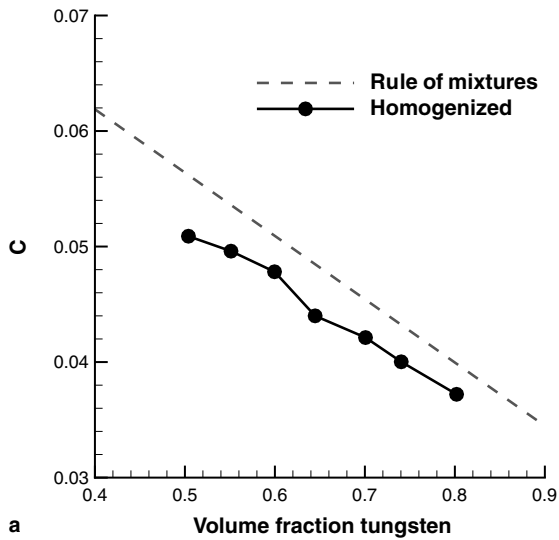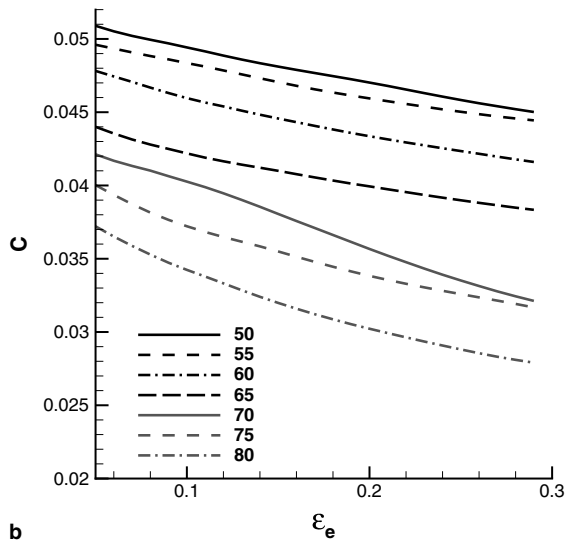
Fig. 8. (a) Strain-rate hardening coefficient C as a function of volume fraction of tungsten particulates. (b) Strain-rate hardening exponent C as a function of effective plastic strain for different volume fractions of tungsten particulates.

temperature versus strain. There is a slight increase in the melting temperature with strain, possibly for reasons similar to the strain-rate hardening case above.

4.6.5. Thermal conductivity

Fig. 10(a) shows the thermal conductivity as a function of the volume fraction of W particulates. The top and the bottom surfaces of each RVE were held at constant
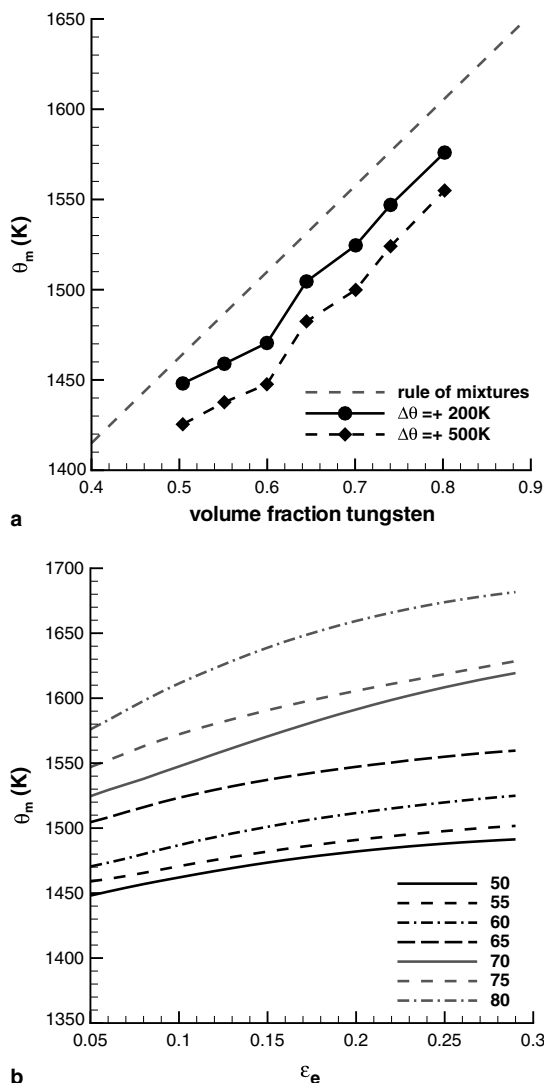
Fig. 9. (a) Melting temperature θ_m as a function of volume fraction of tungsten particulates. (b) Melting temperature θ_m as a function of effective plastic strain for different volume fractions of tungsten particulates.

temperatures, with the top surface held at $+100$ K over the bottom surface. The average heat flux in the X_2-direction was calculated at multiple values of $X_2 = $ constant using the local material parameters; this heat flux was nearly constant throughout the body after reaching steady-state conditions. The average heat flux divided by the overall temperature gradient (100 K/0.25 mm) gave the values reported in Fig. 10(a). The values so obtained are compared with those from the rule of mixtures and also with those computed from the relation given by Hatta and Taya (1985).
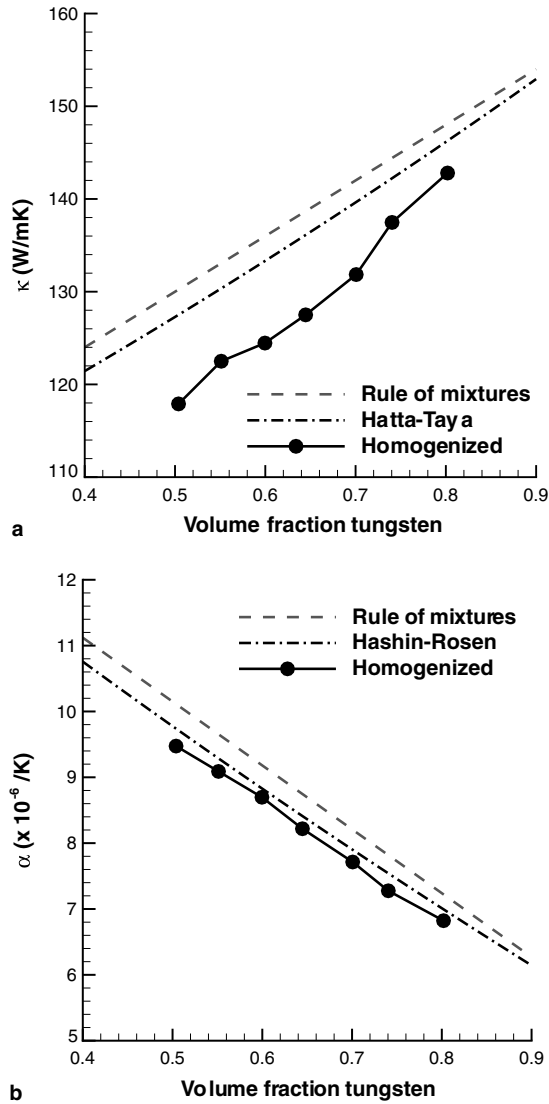
Fig. 10. (a) Thermal conductivity κ as a function of volume fraction of tungsten particulates. (b) Coefficient of thermal expansion $\hat{\alpha}$ as a function of volume fraction of tungsten particulates.

It should be noted that each RVE was tested at both normal orientation and after a 90° rotation. For the W/NiFe RVEs, the rotation made a little difference in the results because of the small difference in the thermal conductivities of the two materials. Care must be taken when implementing this technique for systems with great disparity between the thermal conductivities of the constituents; thermally isotropic arrangements of such systems can be difficult to realize.

4.6.6. Coefficient of thermal expansion

The coefficient of thermal expansion as a function of volume fraction of tungsten is given in Fig. 10(b). The edges of each RVE were held fixed as the body was given a uniform temperature rise of 50 K. The average values of stress components were calculated as indicated in Section 3, and the effective value of the coefficient of thermal expansion was computed by Eq. (37). It should be noted that the effective value of the bulk modulus used in Eq. (37) is obtained from the values of Young's modulus in Fig. 6 and Poisson's ratio of 0.29. The average stress σ_{33} is slightly different from that of the in-plane stresses σ_{11} and σ_{22} due to the cylindrical particulates required by the plane-strain condition; however, the impact on the results is negligible. Note the excellent agreement between the present results and those of the approach proposed by Hashin and Rosen (1970).

4.6.7. Summary of effective material parameters

Eqs. (40) through (48) give the homogenized material parameters as functions of the volume fraction of tungsten, v_f. A polynomial of sufficient order was used for the least squares fit to capture the values. *Note that these relations are only valid for* $0.5 \leqslant v_f \leqslant 0.8$.

$$\text{Young's modulus (GPa): } E = 241.76 + 155.03v_f + 4.53v_f^2, \tag{40}$$

$$\text{Poisson's ratio: } v = 0.29, \tag{41}$$

$$\text{Yield stress (GPa): } A^* = 0.6384 + 0.8985v_f, \tag{42}$$

$$\text{Strain hardening coefficient (GPa): } B^* = 2.394 - 1.152v_f, \tag{43}$$

$$\text{Strain hardening exponent: } n = 0.2126 - 0.1535v_f, \tag{44}$$

$$\text{Strain – rate hardening coefficient: } C = 0.07563 - 0.04794v_f, \tag{45}$$

$$\text{Thermal conductivity (W/mK): } \kappa = 76.24 + 81.63v_f, \tag{46}$$

$$\text{Coefficent of thermal expansion } (\times 10^{-6}/\text{K}): \alpha = 14.11 - 9.138v_f, \tag{47}$$

$$\text{Melting temperature (K): } \theta_m = 1214.1 + 447.1v_f. \tag{48}$$

Listed in Table 5 are the maximum deviations of the effective values of each thermomechanical parameter from those computed with the rule of mixtures and corresponding micromechanical models.

4.7. Verification of the effective values

In order to test the accuracy of the proposed method, a homogeneous material with material parameters found from the above techniques was subjected to a plane-strain tension test at 50,000/s with a uniform temperature rise of 200 K. The stress–strain curve was compared with a similar analysis performed on an RVE. Shown in Fig. 11 is the result for the 80% volume fraction of tungsten particulates. The result of a similar test on a homogeneous material with the properties derived by the rule of mixtures is given for comparison. Note that the maximum point-to-point error for the homogenized material over the entire range of strains is 1.8%. For the seven different volume fractions, the maximum point-to-point error was 2.2%, with

Table 5
Maximum deviation of the homogenized material parameters from the rule of mixtures and micromechanical models

Quantity	Max. % deviation from the rule of mixtures	Micromechanical model	
		Name	Max. % deviation
E	−2.2%	Mori–Tanaka	1.2%
A^*	–	Suquet	5.9%
B^*	6.2%	–	–
n	13.7%	–	–
C	−10.4%	–	–
θ_m	−2.7%	–	–
κ	−10.5%	Hatta–Taya	−8.1%
α	−7.4%	Hashin–Rosen	−3.7%

Fig. 11. Effective stress versus effective strain curve for 80% volume fraction tungsten RVE and its equivalent homogeneous material deformed in plane strain tension.

the average point-to-point error being less than 0.5%. This level of accuracy is encouraging considering that the RVE is not truly isotropic due to the plane strain assumption.

4.7.1. Loading and unloading

During a general loading, material points may be loaded, unloaded, and possibly reloaded. To test the accuracy of the proposed procedure, a RVE containing 60% volume fraction of tungsten particulates and its equivalent homogeneous sample were subjected to the plane strain deformations with the lateral edges kept traction free. However, the prescribed velocity on the upper surface had a non-constant profile, as in Eq. (49).

$$v_2 = \begin{cases} 12.5 \times 10^6 t \;\; \text{m/s}, \quad 0 \leqslant t \leqslant 1 \;\mu\text{s}, \\ 12.5 \;\text{m/s}, \quad 1 < t \leqslant 6 \;\mu\text{s}, \\ 12.5(7 - 10^6 t) \;\text{m/s}, \quad 6 < t \leqslant 8 \;\mu\text{s}, \\ -12.5 \;\text{m/s}, \quad t \geqslant 8 \;\mu\text{s}, \;\text{on} \; X_2 = H. \end{cases} \quad (49)$$

The time t in Eq. (49) is in seconds. The steady axial velocity $v_0 = 12.5$ m/s corresponds to a nominal axial strain-rate of 50,000/s. Shown in Fig. 12(a) is a plot of the effective stress versus time for both the homogeneous sample and the RVE. Note the excellent agreement, even after the body has been unloaded and then reloaded.

4.7.2. Simple shear

The effective material parameters are only accurate if the response of the homogeneous material compares well to that of the RVE under different types of loading. To test the proposed technique, a 60% volume fraction tungsten RVE and a homogeneous sample with the homogenized properties are subjected to a simple shear test. The upper and lower surfaces are restrained in the x_2-direction and the upper surface is given velocity v_0 in the x_1-direction while the lower surface is given the velocity $-v_0$ in the x_1-direction. Here, v_0 was chosen such that the effective strain-rate is 25,000/s. The lateral edges $x_1 =$ constant were kept traction free. Fig. 12(b) shows time-histories of the driving force (the force in the x_1-direction on the upper surface) for the two cases. Note the excellent agreement between the two sets of curves.

4.8. Axisymmetric deformations

This provides a more severe test of values of the effective thermophysical parameters of the homogenized material since tungsten particulates now are in the form of circular rings rather than cylinders. Fig. 13 exhibits the time histories of the axial load required to pull a cylinder containing 60% volume fraction of W particulates at a nominal axial strain rate of 50,000/s. It is clear that loads computed from deformations of the RVE and the homogenized material essentially coincide with each other.

5. Determination of material parameters from the solution of initial-boundary-value problems

In contrast to the approach adopted here, Batra and Kim (1990) used the semi-inverse method to find values of material parameters for a thermoelastoviscoplastic material from a given shear stress–shear strain curve for a steel. They used handbook values of the mass density, Young's modulus, Poisson's ratio, specific heat and thermal conductivity, and estimated values of A, B, C, m, n, and $\dot{\varepsilon}_0$. The initial-boundary-value problem describing coupled thermomechanical deformations was solved numerically. It was postulated that the problem formulation simulates well the test conditions. Values of A, B, C, m, n, and $\dot{\varepsilon}_0$ were iterated upon till the computed shear
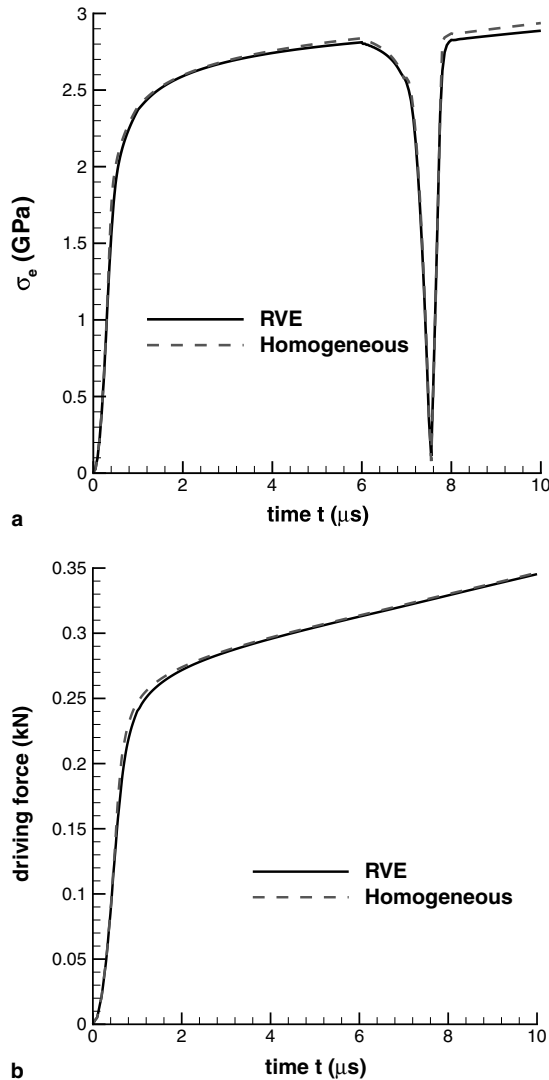
Fig. 12. (a) Effective stress versus time for plane strain tension unload/reload test for 60% volume fraction of tungsten RVE and its equivalent homogeneous material. (b) Driving force versus time in simple shear test for both 60% volume fraction of tungsten RVE and its equivalent homogeneous material.

stress–shear strain curve upto the peak in the shear stress was "close" to that obtained from the test data. They used the same procedure to ascertain values of material parameters in the Bodner–Partom relation (1975), power law, and the Litonski (1977) relation for simple and dipolar (strain-rate gradient dependent) materials. This approach was not tried here. However, present results suggest that a good set of starting values for the iterative process can be estimated from the rule of mixtures.
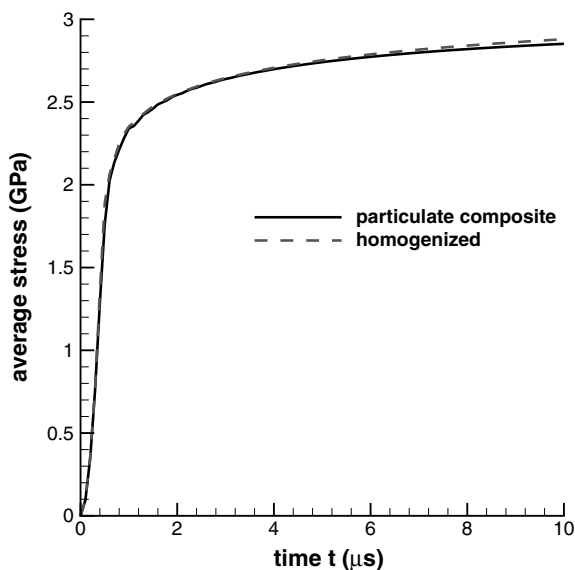
Fig. 13. Time histories of the average axial stress required to pull a circular cylinder having 60% volume fraction of tungsten and its equivalent homogenized material.

6. Local deformation fields

For an ordered arrangement of 50% volume fraction of 50 μm diameter W particulates in the NiFe matrix exhibited in Fig. 14(a), Fig. 14(b) evinces the evolution of the effective plastic strain at three points; one of these points is in the W particulate and the other two are in the NiFe matrix. The specimen is deformed isothermally in plane strain tension at a nominal axial strain rate of 5000/s. Qualitatively similar results are obtained for a random distribution of W particulates. For $t \leqslant 44$ μs, the effective plastic strain at the point in W has the smallest value out of three values. However, for $60 \geqslant t > 44$ μs the effective plastic strain at the point in the W particulate has a value intermediate between those at the two NiFe points. It is clear that the ratio of the effective plastic strain in NiFe to that in W varies with time t. Furthermore, the effective plastic strain and the effective plastic strain rate at the two points in the NiFe matrix are quite different. As expected, deformations of W and NiFe are inhomogeneous.

Fig. 14(c) exhibits the time history of the effective plastic strain averaged over the W, the NiFe and the entire body. Note that the effective plastic strain is non-negative. At any time $t > 4$ μs the averaged effective plastic strain in the NiFe matrix is greater than that in the W particulates because the former has a lower yield stress than the latter. From these averaged values of the effective plastic strain, $\varepsilon_{e,avg}^{p}$, a pseudo-effective stress, σ_{eff}^{ps}, is computed in each constituent from the relation

$$\sigma_{eff}^{ps} = A + B(\varepsilon_{e,avg}^{p})^{n}, \tag{50}$$
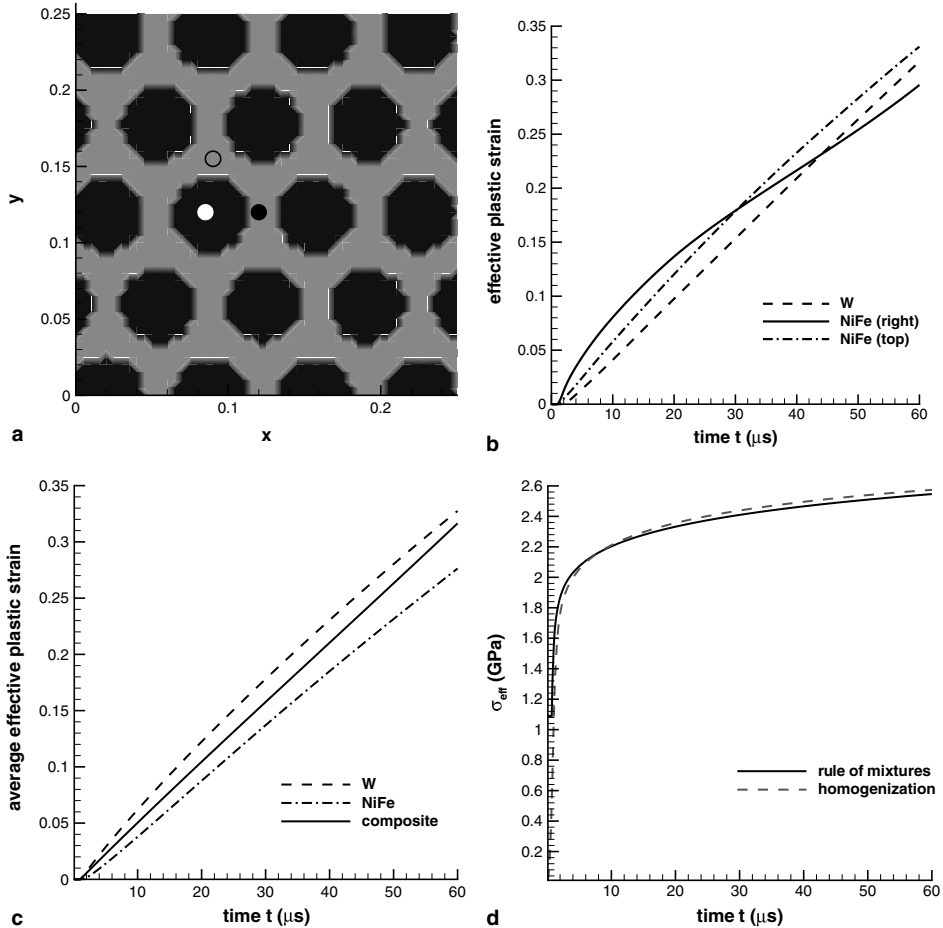
Fig. 14. (a) Ordered distribution of W particulates in the NiFe matrix, (b) time histories of the evolution of the effective plastic strain at three points, (c) time histories of the effective plastic strain averaged over W, NiFe and the entire body, and (d) comparison of the effective stress versus time computed from the rule of mixtures with that from surface tractions acting on the bounding surfaces.

where A, B and n are material constants in the Johnson–Cook relation. The rule of mixture is applied to the pseudo-effective stresses to compute the effective stress in the composite. The time history of the effective stress so computed is compared in Fig. 14(d) with that obtained from the surface tractions needed to deform the body. It is clear that at every time t, the effective stresses computed by the two methods are very close to each other even though the effective plastic strain does not obey the rule of mixtures (cf. Fig. 14(c)) for large values of time t.

In an attempt to see if the above-mentioned technique can be generalized to a composite of three constituents we have analyzed deformations of a composite comprised of 375% volume fraction of 50 μm diameter W particulates and 17.14%

volume fraction of 30 μm diameter steel particulates embedded in NiFe matrix. The random distribution of particulates is exhibited in Fig. 15(a), and the effective stress versus effective plastic strain curves for the three constituents are depicted in Fig. 15(b). It is clear that the three materials strain-harden at very different rates. Time histories of the evolution of the effective plastic strain at three points, one in each material, on the horizontal line $X_2 = 0.12$ mm in the reference configuration are shown in Fig. 15(c). These evince quite different effective plastic strain histories at the three points. Because of varying deformations, these points need not lie on a horizontal line at all times. The plot of Fig. 15(d) reveals that at any time t the effective stress computed with the rule of mixture from the pseudo-effective stress
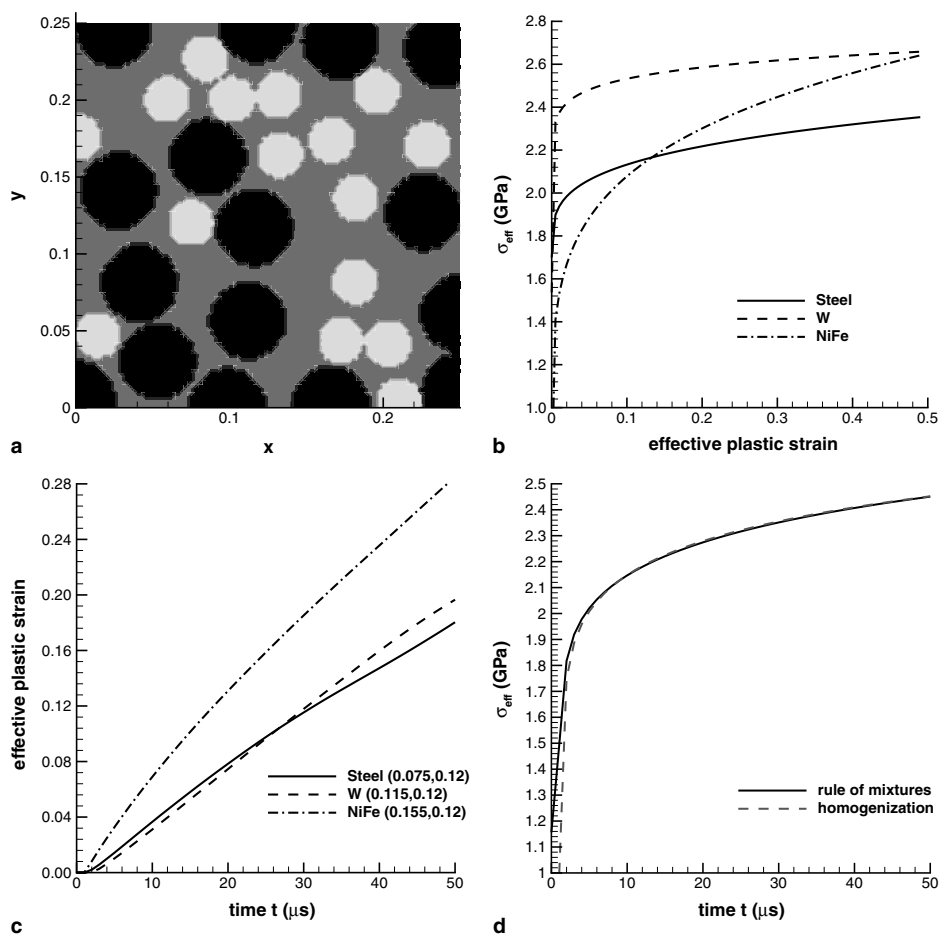
Fig. 15. (a) Random distribution of W (dark) and steel (light grey) particulates in the NiFe matrix, (b) effective stress versus effective strain curves for each constituent, (c) time histories of the effective plastic strain at a point in each constituent, and (d) comparison of the effective stress versus time computed from the rule of mixtures with that from surface tractions acting on the bounding surfaces.

in each constituent matches very well with that obtained from surface tractions acting on the bounding surfaces of the specimen. It is a nontrivial task to find time histories of the average values of the effective plastic strain in each constituent.

In the aforestated results mechanical and thermal deformations have been considered separately from each other. Coupled thermomechanical deformations of the composite have been scrutinized by Batra and Love (2005a,b, 2004) both by homogenizing the material and by considering deformations of each constituent. Thermal stresses are induced because of different values of thermophysical parameters of the two constituents. When the composite was replaced by an equivalent homogenized medium the criterion to delineate the initiation of localization of deformation proposed for a homogeneous material (e.g., see Batra and Kim (1992), Batra and Lear (2005)) could be used. However, when deformations of each constituent were analyzed, this criterion did not give a coherent shear band. Furthermore, the criterion was satisfied at a material point at time t_1 but failed at the same material point at time $t_2 > t_1$. Eventually a contiguous narrow region formed in which the energy dissipation rate due to plastic working is considerably more than that in the material surrounding it. Since the analysis of deformations of each constituent is computationally very expensive, Batra and Love (2005c) used a multiscale analysis technique to delineate the localization of deformation into narrow bands. Attempts to improve upon the multiscale analysis are being pursued.

7. Conclusions

We have developed a technique to find the thermoelastoviscoplastic properties of a metal-metal particulate composite. This technique was used to find the thermoviscoplastic parameters for the Johnson–Cook relation for a tungsten heavy alloy composed of tungsten particles perfectly bonded to a nickel–iron matrix. It was found that the rule of mixtures underpredicts the strain hardening parameters B^* and n, with the underprediction of n being as much as 13%. Furthermore, the strain-rate hardening coefficient C was shown to vary with strain, possibly due to the two constituents being strained at different rates. The rule of mixtures over-predicts C by ~10%. The thermal softening of the homogenized material, governed by the pseudo-melting temperature θ_m was found to be slightly less than that predicted by the rule of mixtures. A slight (<5%) variation in the melting temperature at different strains and temperature ranges was observed.

The values of effective parameters were verified by subjecting a representative volume element of the microstructure and the corresponding homogeneous material to a series of tests. A tension test where the specimen was unloaded and reloaded, a simple shear test, and a test involving axisymmetric deformations showed that the stress strain curves of the homogenized sample and the RVE were nearly identical.

Time histories of the evolution of the effective plastic strain at a point in each constituent reveal significant differences in deformations of the two constituents. Averaged values of the effective plastic strain in a constituent are used to find the pseudo-effective stress in that constituent from its stress–strain relation. The effective

stress in the two or the three constituent composite computed from the pseudo-effective stresses and the rule of mixture is found to match well with that found from surface tractions acting on the specimen boundaries.

Acknowledgement

References

Aboudi, J., Pindera, M.-J., Arnold, S.M., 2001. Higher-order theory for periodic multiphase materials with inelastic phases. Int. J. Plasticity 12, 805–847.

Batra, R.C., Love, B.M., 2005a. Crack propagation due to brittle and ductile failures in microporous thermoelastoviscoplastic functionally graded materials. Eng. Fract. Mech. 72, 1954–1979.

Batra, R.C., Love, B.M., 2005b. Mesoscale analysis of shear bands in high strain rate deformations of tungsten/nickel–iron composites. J. Thermal Stresses 28, 747–782.

Batra, R.C., Love, B.M., 2005c. Multiscale analysis of adiabatic shear bands in tungsten heavy alloy particulate composites. Int. J. Multiscale Comput. Eng. (accepted).

Batra, R.C., Love, B.M., 2004. Adiabatic shear bands in functionally graded materials. J. Thermal Stresses 27, 1101–1123.

Batra, R.C., Lear, M.H., 2005. Adiabatic shear banding in plane strain tensile deformations of 11 thermoviscoplastic materials with finite wave speed. Int. J. Plasticity 21, 1521–1545.

Batra, R.C., Liang, X.Q., 1997. Finite deformations of smart structures. Comput. Mech. 20, 427–438.

Batra, R.C., Kim, C.H., 1992. Analysis of shear bands in twelve materials. Int. J. Plasticity 8, 425–452.

Batra, R.C., Kim, C.H., 1990. Effect of viscoplastic flow rules on the initiation and growth of shear bands at high strain rates. J. Mech. Phys. Solids 38, 859–874.

Batra, R.C., 1975. On heat conduction and wave propagation in non-simple rigid solids. Lett. Appl. Eng. Sci. 3, 97–107.

Bodner, S.R., Partom, Y., 1975. Constitutive equations for elastic-viscoplastic strain-hardening materials. J. Appl. Mech. 56, 385–389.

Ponte Castañeda, P., 1996. Exact second order estimates for the effective mechanical properties of nonlinear composites. J. Mech. Phys. Solids 44, 827–862.

Ponte Castañeda, P., 2002. Second-order homogenization estimates for nonlinear composites incorporating field fluctuations: I – theory. J. Mech. Phys. Solids 50, 737–757.

Cattaneo, C., 1958. A form of the heat equation which eliminates the paradox of instantaneous propagation. C. R. Acad. Sci. 247, 431–433.

Chaboche, J.L., Kanouté, P., Roos, A., 2005. On the capabilities of mean-field approaches for the description of plasticity in metal matrix composites. Int. J. Plasticity 21, 1409–1434.

Chaboche, J.L., Kruch, S., Maire, J.F., Pottier, J., 2001. Towards a micromechanics based inelastic and damage modeling of composites. Int. J. Plasticity 17, 411–439.

Chester, M., 1963. Second sound in solids. Phys. Rev. 131, 2013–2015.

Christensen, R.M., Lo, K.H., 1979. Solution for effective shear properties of three phase sphere and cylinder models. J. Mech. Phys. Solids 27, 315–330.

Dai, L.H., Liu, L.F., Bai, Y.L., 2004. Effect of particle size on the formation of adiabatic shear bands in particle reinforced metal-matrix composites. Mater. Lett. 58, 1773–1776.

Doghri, I., Friebel, C., 2005. Effective elasto-plastic properties of inclusion-reinforced composites; study of shape, orientation, and cyclic response. Mech. Mater. 37, 45–68.

Dvorak, G.J., 2000. Composite materials: inelastic behavior, damage, fatigue and fracture. In. J. Solids Struct. 37, 155–170.

Dvorak, G.J., Srinivas, M.V., 1999. New estimates of overall properties of heterogeneous solids. J. Mech. Phys. Solids 47, 899–920.

Dvorak, G.J., 1992. Transformation field analysis of inelastic composite materials. Proc. R. Soc. Lond. A 431, 89–110.

Fotiu, P.A., Nemat-Nasser, S., 1996. Overall properties of elastic-viscoplastic periodic composites. Int. J. Plasticity 12 (2), 163–190.

Fröhlich, H., Sack, R., 1946. Theory of the rheological properties of dispersions. Proc. Roy. Soc. A 185, 415–430.

Hashin, Z., Shtrikman, S., 1963. A variational approach to the theory of elastic behavior of multiphase materials. J. Mech. Phys. Solids 11, 127–140.

Hashin, Z., Rosen, B.W., 1970. Effective thermal expansion coefficients and specific heats of composite materials. Int. J. Eng. Sci. 8, 157–173.

Hatta, H., Taya, M., 1985. Effective thermal conductivity of a misoriented short fiber composite. J. Appl. Phys. 58, 2478–2486.

Hughes, T.J.R., 1987. Finite Element Method. Prentice-Hall, Englewood Cliffs, NJ.

Jiang, B., Batra, R.C., 2002. Effective properties of a piezocomposite containing shape memory alloy and inert inclusions. Continuum Mech. Thermodyn. 14, 87–111.

Jiang, B., Batra, R.C., 2001a. Micromechanical modeling of a composite containing piezoelectric and shape memory alloy inclusions. J. Intell. Mater. Syst. 12, 165–182.

Jiang, B., Batra, R.C., 2001b. Effective electroelastic properties of a piezocomposite with viscoelastic and dielectric relaxing matrix. J. Intell. Mater. Syst. 12, 847–866.

Johnson, G.R., Cook, W.H., 1983. A constitutive model and data for metals subjected to large strains, high strain-rates, and high temperatures. In Proc. 7th Int. Symp. on Ballistics, 541–547.

Kachanov, M., Sevostianov, I., 2005. On quantitative characterization of microstructures and effective properties. Int. J. Solids Struct. 42, 309–336.

Litonski, J., 1977. Bulletin de l'Academie Polonaise des Sciences. Sci. Tech. 25, 7–15.

Liu, X.N., Hu, G.K., 2005. A continuum micromechanical theory of overall plasticity for particulate composites including particle size effect. Int. J. Plasticity 221, 777–799.

Mori, T., Tanaka, K., 1973. Average stress in matrix and average elastic energy of materials with misfitting inclusions. Acta Metall. 21, 571–574.

Nemat-Nasser, S., Hori, M., 1993. Micromechanics: Overall Properties of Heterogeneous Materials. Elsevier, Amsterdam.

Ohno, N., Matsuda, T., Wu, X., 2001. A homogenization theory for elastic-viscoplastic composites with point symmetry of internal distributions. Int. J. Solids Struct. 38, 2867–2878.

Paley, M., Aboudi, J., 1992. Micromechanical analysis of composites by the generalized method of cells. Mech. Mater. 14, 127–139.

Pindera, M.-J., Freed, A.D., Arnold, S.M., 1993. Effects of fiber and interfacial layer morphologies on the thermoplastic response of metal matrix composites. Int. J. Solids Struct. 30 (9), 1213–1238.

Pindera, M.J., Aboudi, J., 1988. Micromechanical analysis of yielding of metal matrix composites. Int. J. Plasticity 4 (3), 195–214.

Pierard, O., Doghri, I., 2006. An enhanced affine formulation and the corresponding numerical algorithms for the mean-field homogenization of elasto-viscoplastic composites. Int. J. Plasticity 22, 131–157.

Sun, L.Z., Ju, J.W., 2004. Elastoplastic modeling of metal matrix composites containing randomly located and oriented spheroidal particles. J. Appl. Mech. 71, 774–785.

Suquet, P., 1993. Overall potential and extremal surfaces of power law or ideally plastic composites. J. Mech. Phys. Solids 41, 981–1002.

Talbot, D.R.S., Willis, J.R., 1985. Variational principles for inhomogeneous nonlinear media. IMA J. Appl. Math. 35, 39–54.

Vernotte, P., 1958. The true heat equation. C. R. Acad. Sci. 247, 2103.

Walker, K.P., Freed, A.D., Jordan, E.H., 1994. Thermoviscoplastic analysis of fibrous periodic composites by the use of triangular subvolumes. Compos. Sci. Technol. 50 (1), 71–84.

Weng, G.J., 1984. Some elastic properties of reinforced solids, with special reference to isotropic ones containing spherical inclusions. Int. J. Eng. Sci. 22, 8485–8856.

Wilkinson, D.S., Wolfgang, P., Oeschner, M., 2001. Modeling the mechanical behavior of heterogeneous multi-phase materials. Prog. Mater. Sci. 46, 379–405.

Willis, J.R., 1993. The overall elastic response of composite materials. J. Appl. Mech. 50, 1202–1209.